BIOCHEMISTRY
including biophysical chemistry & molecular biology

Article

pubs.acs.org/biochemistry

A Heme Peroxidase with a Functional Role as an L-Tyrosine Hydroxylase in the Biosynthesis of Anthramycin

Katherine L. Connor,[†] Keri L. Colabroy,[§] and Barbara Gerratana*[,†]

[†]Department of Chemistry and Biochemistry, University of Maryland, Maryland 20742, United States

[§]Department of Chemistry, Muhlenberg College, Allentown, Pennsylvania 18014, United States

Supporting Information

ABSTRACT: We report the first characterization and classification of Orf13 (*S. refuineus*) as a heme-dependent peroxidase catalyzing the *ortho*-hydroxylation of L-tyrosine to L-DOPA. The putative tyrosine hydroxylase coded by *orf13* of the anthramycin biosynthesis gene cluster has been expressed and purified. Heme b has been identified as the required cofactor for catalysis, and maximal L-tyrosine conversion to L-DOPA is observed in the presence of hydrogen peroxide. Preincubation of L-tyrosine with Orf13 prior to the addition of hydrogen peroxide is required for L-DOPA production. However, the enzyme becomes inactivated by hydrogen peroxide during catalysis. Steady-state kinetic analysis of L-tyrosine hydroxylation revealed similar catalytic efficiency for both L-tyrosine and hydrogen peroxide. Spectroscopic data from a reduced-CO(g) UV−vis spectrum of Orf13 and electron paramagnetic resonance of ferric heme Orf13 are consistent with heme peroxidases that have a histidyl-ligated heme iron. Contrary to the classical heme peroxidase oxidation reaction with hydrogen peroxide that produces coupled aromatic products such as *o,o′*-dityrosine, Orf13 is novel in its ability to catalyze aromatic amino acid hydroxylation with hydrogen peroxide, in the substrate addition order and for its substrate specificity for L-tyrosine. Peroxygenase activity of Orf13 for the *ortho*-hydroxylation of L-tyrosine to L-DOPA by a molecular oxygen dependent pathway in the presence of dihydroxyfumaric acid is also observed. This reaction behavior is consistent with peroxygenase activity reported with horseradish peroxidase for the hydroxylation of phenol. Overall, the putative function of Orf13 as a tyrosine hydroxylase has been confirmed and establishes the first bacterial class of tyrosine hydroxylases.

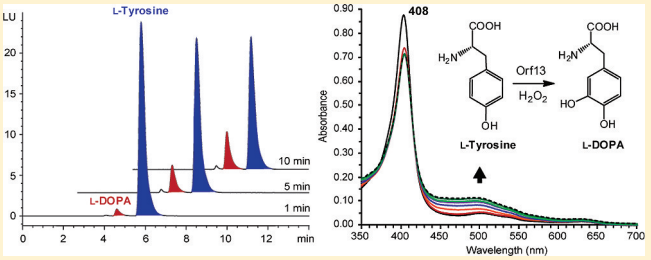

Pyrrolo[1,4]benzodiazepines (PBDs), lincosamides, and hormaomycin are three classes of natural products from actinomycetes, which have antimicrobial and/or antitumor activities due to their different chemical properties (Figure 1A). PBDs are sequence selective DNA alkylating compounds that inhibit transcription and replication processes,[1] lincosamides disrupt and inhibit protein synthesis,[2] and hormaomycin is a despipeptide with potent narrow-spectrum antibiotic activity.[3] PBDs, lincosamides, and hormaomycin share a common hydropyrrole moiety that originates from the same metabolic precursor, L-tyrosine.[4−6] The tyrosine to hydropyrrole transformation is unique to the biosynthesis of these natural products and has remained largely uncharacterized. Putative assignment of the tyrosine hydroxylase and DOPA-dioxygenase activities proposed to be involved in the first two steps of this transformation is originally based on cell free extract studies of enzymes from the lincomycin A biosynthetic pathway[7] (Figure 1B). Formation of the cyclized imine (**4a**) from L-tyrosine was observed using cell free extract from coexpression of the putative tyrosine hydroxylase (LmbB2) and DOPA-dioxygenase (LmbB1).[8,9] LmbB1 alone converted L-DOPA to the same cyclic product (**4a**), suggesting that LmbB2 and its homologues Orf13, TomI, SibU, and HrmE from the anthramycin, tomaymycin, sibiromycin, and hormaomycin biosynthetic pathways,[6,10−12] respectively, are the putative tyrosine hydroxylase catalyzing the first step of this unprecedented transformation.

The chemical reaction of L-tyrosine to L-DOPA is an *ortho*-hydroxylation of an aromatic ring. Enzymes performing aromatic hydroxylation are recognized as monophenol monooxygenases and have been described in five different classes based on their cofactor requirement. These are the heme dependent cytochrome P450 enzymes and peroxidases,[13] di-iron hydroxylases,[14] non-heme iron pterin or α-ketoglutarate dependent monooxygenases,[15] type III non-heme copper dependent monooxygenases,[16] and the metal free flavin dependent monooxygenases.[17] Within the five classes of monophenol monooxygenases, non-heme iron pterin or α-ketoglutarate dependent enzymes have highly conserved 2-His-1-carboxylate triad catalytic motifs[18] and catalyze the *ortho*-hydroxylation of L-tyrosine to L-DOPA.[15,16] A BLAST search of the putative tyrosine hydroxylase homologues identifies only one other statistically significant protein, AMED_5527 from actinobacteria, which is also uncharacterized. The sequences of

Received: July 26, 2011
Revised: September 12, 2011
Published: September 15, 2011

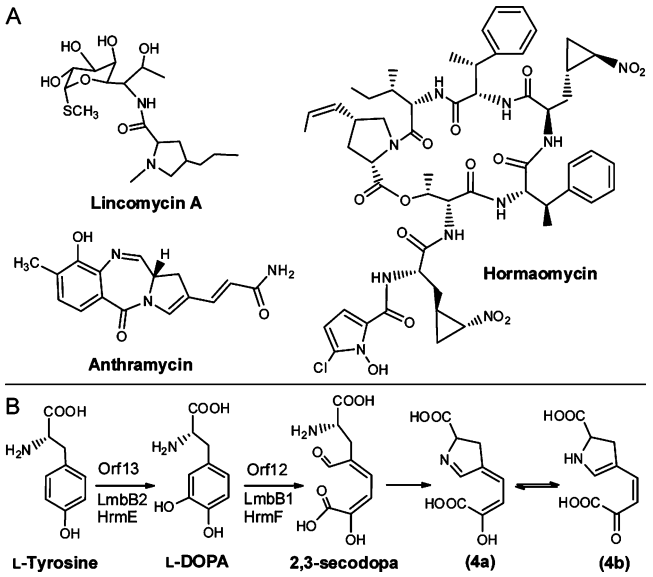

Figure 1. (A) The natural products lincomycin A, anthramycin (a PBD), and hormaomycin. (B) The initial steps proposed for the biosynthesis of the hydropyrrole moiety found in lincomycin A, PBDs, and hormaomycin. *Ortho*-hydroxylation of L-tyrosine to L-DOPA by Orf13 (*S. refuineus*), LmbB2 (*S. lincolnesis*), or HrmE (*S. griseoflavus*) is the first step of hydropyrrole moiety biosynthesis in the natural products anthramycin, lincomycin A, and hormaomycin, respectively.

these six homologues do not contain any known conserved domains or conserved motifs (Figure S1). This poses an intriguing question as to the cofactor requirement for this putative tyrosine hydroxylase. It may require an already established cofactor for monophenol monooxygenase activity, a new cofactor or have no cofactor requirement at all. In all cases, this enzyme likely represents a new class performing aromatic hydroxylation and oxidation reactions.

Presented here is the biochemical, biophysical, and kinetic characterization of the putative tyrosine hydroxylase Orf13. These data confirm the functional assignment of these enzymes as tyrosine hydroxylases and establish their classification as heme dependent peroxidases. To the best of our knowledge, this represents the first functional identification of a bacterial tyrosine hydroxylase, in addition to the first heme peroxidase that can utilize hydrogen peroxide for aromatic amino acid hydroxylation.

EXPERIMENTAL PROCEDURES

Materials and Methods. All purification resins and protein molecular weight standards for the quaternary structure determination were purchased from G.E. Healthcare (Piscataway, NJ). The pET24a vector was purchased from Novagen (Darmstadt, Germany), and the pCW vector and RP523 *E. coli* strain were generously donated by Prof. Michael A. Marletta (UC-Berkeley). Fermentas (Glen Burnie, MD) mini-prep kit was used for DNA purification. Sodium phosphate, imidazole, sodium dithionite, and hydrogen peroxide (30% solution) were purchased with the highest purity from ThermoFisher Scientific (Fair Lawn, NJ). Dithiothreitol (DTT) was purchased from American Bioanalytical Inc. (Natick, MA). Catalase, superoxide dismutase (SOD), and all other chemicals were purchased with the highest purity from Sigma-Aldrich (St. Louis, MO). The Orf13 extinction coefficient was calculated by performing quantitative amino acid analysis (AAA Service Laboratory; Damascus, OR) for triplicate samples with measured A_{280} values. Metal analysis of Orf13 by inductively coupled plasma mass spectrometry (ICP-MS) was performed in the Department of Geological Sciences at Michigan State University (East Lansing, MI). High performance liquid chromatography was performed with an Agilent 1000 Series HPLC (Foster City, CA) equipped with 1100 Series multiple wavelength and 1200 Series fluorescence detectors. All UV−vis absorption spectra or measurement of catechol−nitrite complexes for kinetic assays were obtained with a Varian UV−vis Cary100 spectrophotometer with temperature controller (Walnut Creek, CA). Electrospray Ionization mass spectrometry with tandem mass spectrometry (ESI-MS/MS) was performed with an LTQ Orbitrap XL (Thermo Scientific; San José, CA). Anaerobic experiments were performed in an 830-ABC series compact glovebox (PLAS-LABORATORIES, Inc.; Lansing, MI) equipped with a Model 10 gas analyzer and digital heated fan box with palladium catalyst bed (Coy Laboratory Products, Inc.; Grass Lake, MI).

Cloning of Native (Non-Fusion-Tagged) Orf13. The gene encoding Orf13 was amplified by PCR from the p-ANT-1 cosmid containing the anthramycin gene cluster constructed by Dr. Wei Li in our laboratory (unpublished results). NdeI and *Hin*dIII restriction sites were incorporated into the primers for insertion into the pET24a vector. Amplified *orf13* was digested with NdeI and *Hin*dIII, ligated into the pET24a vector, and transformed into GeneHogs (Invitrogen; Carlsbad, CA). DNA sequencing confirmed correct construction of the pET24a/*orf13* plasmid for the recombinant expression of native Orf13 in BL21(DE3) *E. coli*. The *orf13* gene was also cloned into the pCW vector for recombinant expression in RP523 *E. coli* by digestion of pET24a/*orf13* with *Hin*dIII and NdeI and insertion into the pCW vector cut with the same restriction enzymes. DNA sequencing confirmed the correct construction of pCW/*orf13*.

Expression and Purification of Native Orf13 in BL21(DE3) *E. coli*. Orf13 was expressed in BL21(DE3) *E. coli* cells transformed with pET24/*orf13*. Cells were grown at 37 °C in LB medium with 50 μg/mL kanamycin and induced with D-lactose (0.2% w/v) when the OD at 600 nm reached 0.8−1.0. Cells were harvested 8 h after induction, and the cell pellets were flash frozen in liquid nitrogen and stored at −80 °C until purification. 6 g of cells were lysed by French press, and the cell free extract was loaded onto a 6 mL column of Ni-Sepharose pre-equilibrated with buffer A (50 mM sodium phosphate (pH 8.0), 300 mM NaCl, and 1 mM DTT). The column was washed with 20 column volumes of buffer A containing 20 mM imidazole at 1 mL/min at 4 °C. Orf13 was eluted with 3 column volumes of buffer A containing 70 mM imidazole and fractions containing the enzyme were pooled and concentrated using a filtration membrane Amicon (30 kDa MWCO) by centrifugation (Millipore, Billerica, MA) to a concentration of 10 mg/mL. The concentrated enzyme solution was then loaded onto a S-200 HR column (2.5 × 40 cm; 196 mL column volume) pre-equilibrated with buffer B (10 mM imidazole, 50 mM sodium phosphate (pH 8.0), 300 mM NaCl, and 10% glycerol) and eluted at 0.4 mL/min. Fractions containing Orf13 were pooled and concentrated to at least 10 mg/mL as previously described, flash frozen by liquid nitrogen in liquid droplets, and stored at −80 °C. Purity of Orf13 was greater than 95% as judged by SDS-PAGE (Figure S2A). The protein concentration was determined using the experimentally determined extinction coefficient ε_{280} 2.8 ± 0.2 mL mg^{-1} cm^{-1}

(pH 8.0, 25 °C) with final purification yields of 2−3 mg of Orf13 per gram of cells lysed. An alternative purification method for Orf13 by anionic exchange chromatography was also developed. 6 g of cells were lysed by French press, and the cell free extract was loaded onto a Q-Sepharose column (2.5 × 49 cm; 240 mL column volume) pre-equilibrated with buffer A (50 mM sodium phosphate (pH 8.0), 30 mM NaCl, 50 mM DTT, and 10% glycerol). The column was washed with 3 column volumes of buffer A at 2 mL/min at 4 °C, followed by a salt gradient of 30−600 mM NaCl within 1.2 L. Orf13 eluted between 120 and 150 mM NaCl of the linear gradient and fractions containing the enzyme were pooled and concentrated to 10 mg/mL as previously described. Gel filtration S-200HR chromatography was performed as described before with buffer containing 50 mM sodium phosphate (pH 8.0), 300 mM NaCl, 50 mM DTT, and 10% glycerol. Orf13 was obtained with similar yield and purity as in the Ni-Sepharose method (Figure S2B). For all reported specific activity and steady-state kinetic data, Orf13 was purified and stored in buffer B (10 mM imidazole, 50 mM sodium phosphate (pH 8.0), 300 mM NaCl, and 10% glycerol) to maintain stable enzyme with a ferric heme iron oxidation state. Orf13 that had been purified and stored in the presence of 50 mM DTT was buffer exchanged into buffer B at 4 °C using a G-50 column (1 × 5 cm; 4 mL column volume) to remove DTT prior to enzyme assays. Auto-oxidation of the heme iron to the ferric state upon buffer exchange was observed in the Soret band, which shifted from 420 to 405 nm (Figure S3).

Quaternary Structure Determination of Orf13 by Gel Filtration. The oligomeric state of purified Orf13 was determined using a Superdex200 column (1 × 30 cm; 24 mL column volume) pre-equilibrated at 4 °C with 50 mM sodium phosphate (pH 8.0), 150 mM NaCl, and 50 mM DTT at 0.4 mL/min. Molecular weight standards used were ribonuclease A (13.7 kDa), ovalbumin (44 kDa), conalbumin (75 kDa), and aldolase (158 kDa).

High Performance Liquid Chromatography and Mass Spectrometry for Porphyrin Detection and Identification. An HPLC method to detect porphyrins was performed as previously described.[19] Samples (110 μL) of Orf13 and/or standards of heme b (iron protoporphyrin IX) or protoporphyrin IX (PPIX) were incubated at room temperature for 1 h in 2% SDS (w/v). Porphyrins were detected at 405 nm. Heme b and PPIX standards had average retention times of 42 and 44 min, respectively. The peaks observed at 42 and 44 min from the Orf13 sample were collected, treated with formic acid (1% v/v,) and injected at 25 μL/min into an ESI-MS. The parent ions of 616.3 m/z and 563.5 m/z observed in the Orf13 samples at 42 and 44 min, respectively, were selected for fragmentation by collision-induced dissociation. Heme b and PPIX standards were treated and analyzed accordingly.

Heme b Quantitation and Stoichiometry. The pyridine hemochromagen method was performed as described[20] with a UV−vis Cary100 spectrophotometer. A basic pyridine solution containing 50% (v/v) pyridine and 200 mM NaOH was prepared fresh for all analyses. The concentration of heme b from Orf13 samples was calculated with the extinction coefficient 22.1 mM^{-1} cm^{-1} for heme b and the stoichiometric ratio of heme b determined by the molar ratio of heme b to Orf13. All analyses were performed in triplicate.

Electron Paramagnetic Resonance of Orf13. Orf13 with 50% heme b occupancy purified and stored in the presence of 50 mM DTT was buffer exchanged into 20 mM sodium phosphate (pH 8.0) at 4 °C using a G-50 column (1 × 5 cm; 4 mL column volume). Auto-oxidation of heme b to the ferric state was observed after removal of DTT (refer to Figure S3); however, 5 mM ferricyanide was also added to Orf13 to ensure complete oxidization of the heme iron to the ferric state. The ferricyanide was removed by a second G-50 column (1 × 5 cm; 4 mL column volume) pre-equilibrated with 20 mM sodium phosphate (pH 8.0) at 4 °C. The final Orf13 sample was concentrated to 6 mg/mL, diluted 1:1 (v/v) in 100% glycerol (300 μL final volume), transferred to an EPR quartz tube, and flash frozen slowly in liquid nitrogen. The sample was stored at −80 °C until EPR analysis. The EPR spectrum of Orf13 was obtained at The Johns Hopkins University in the Department of Chemistry using a Bruker EMX EPR spectrometer controlled with a Bruker ER 041 X G microwave bridge at 15 K. The instrument was equipped with a continuous-flow liquid helium cryostat (ESR900) coupled to a temperature controller (TC503) made by Oxford Instruments, Inc.

Orf13 Activity Assays with Detection of L-Tyrosine and L-DOPA by HPLC-FLD. Orf13 (2.5 μM) was preincubated in 50 mM sodium phosphate (pH 8.0) containing 15 mM DTT or 15 mM dithionite for 5 min on ice and then incubated for 5 min at 37 °C before addition of L-tyrosine (1 mM final) to start the reaction. In assays testing the requirement of hydrogen peroxide, Orf13 was preincubated with L-tyrosine (1 mM final) for 5 min on ice and 5 min at 37 °C, and then hydrogen peroxide (0.1 mM final) was added to initiate the reaction. All assays were performed at 37 °C up to 15 min in triplicate. Four time point aliquots (75 μL) were quenched with 2.5 M HCl (10 μL), and chloroform (40 μL) was added to the quenched samples, spun for 2 min at 3400 rpm at room temperature. The aqueous layer (65 μL) was transferred to new tube containing 2.5 M NaOH (10 μL). 20 μL from each sample was analyzed by HPLC-FLD as described for the detection of L-tyrosine and L-DOPA.[21] L-Tyrosine and L-DOPA stocks were quantified spectrophotometrically at ε_{275} = 1.4 mM^{-1} cm^{-1} [22] and ε_{280} = 2.63 mM^{-1} cm^{-1},[23] respectively. L-DOPA and L-tyrosine standards had an average retention time of 4.5 and 5.5 min, respectively. The amount of L-DOPA produced by Orf13 was determined based on a calibration curve for L-DOPA made with standard samples quantified spectrophotometrically and treated under the same sample work-up condition described. In Orf13 specific activity assays for the dihydroxyfumaric acid (DHFA) or L-ascorbate dependent reactions, Orf13 (2.5 μM) was preincubated with DHFA (2 mM) or L-ascorbate (25 mM) for 5 min on ice and then 5 min at 37 °C in 100 mM sodium phosphate (pH 8.0). The reaction was initiated by addition of L-tyrosine (5 mM) and carried out for 15 min with time point aliquots quenched, prepared, and analyzed as described above. These assays were performed in triplicate with or without catalase (75 μg/mL) or SOD (100 μg/mL) or were performed in an anaerobic glovebox. L-Ascorbate stocks were quantified spectrophotometrically at ε_{290} = 2.8 mM^{-1} cm^{-1}.[24]

L-DOPA Colorimetric Assay for the Steady-State Kinetics of Orf13 of the Hydrogen Peroxide Dependent Reaction. A discontinuous assay was developed to monitor formation of L-DOPA in the hydrogen peroxide dependent reaction of Orf13 using a colorimetric method as previously described.[25,26] Orf13 (0.3−1 μM; 75% heme b occupancy) was incubated with L-tyrosine for 5 min at 37 °C in 100 mM sodium phosphate (pH 8.0), followed by addition of hydrogen

peroxide to initiate the reaction. Assays were performed in triplicate at 37 °C for 4 min with time points taken at 1, 2, 3, and 4 min in 90 μL aliquots quenched with 2.5 M HCl (10 μL). A solution containing 12.5% (w/v) sodium nitrite and 12.5% (w/v) sodium molybdate (35 μL) was added to the quenched samples and incubated for 10 min at room temperature. NaOH (10 μL, 3 M) was added to the sample, and the L-DOPA−nitrite complex was measured at 500 nm within 10−15 s. A standard curve of L-DOPA from 1 to 100 μM was prepared the same day for each set of assays. L-tyrosine and L-DOPA stocks were quantified as previously described.[22,23] Hydrogen peroxide stocks were prepared fresh and quantified spectrophotometrically at $\varepsilon_{240\ nm}$ = 43.6 M^{-1} cm^{-1}.[24] Fixed variable concentrations of L-tyrosine (125 μM−5 mM) at a fixed concentration of hydrogen peroxide (500 μM) were used to determine the steady-state rate constants for L-tyrosine. Fixed variable concentrations of hydrogen peroxide (100 μM−1 mM) at a fixed concentration of L-tyrosine (2 mM) were used to determine the steady-state rate constants for hydrogen peroxide. The steady-state data for both L-tyrosine and hydrogen peroxide were fit to the Michaelis−Menten equation using the software program Prism 4 (GraphPad) to obtain the steady-state rate constants. Assay controls with a blank solution without Orf13 were used to correct for background. Orf13 background control assays were carried out with the same concentration of enzyme in the absence of substrates. No enzyme background at 500 nm was observed with 1.5 μM Orf13 or less. All controls were run in triplicate and in parallel with assay samples and underwent the same colorimetric work-up described above.

Orf13 Specific Activity Assays with Substrate Analogues. Production of L-tyrosine was monitored by HPLC-FLD as described[21] for assays with L-phenylalanine as the substrate. Orf13 (1.5 μM) was incubated with L-phenylalanine (5 mM final) for 5 min at 37 °C in 100 mM sodium phosphate (pH 8.0) followed by addition of hydrogen peroxide (500 μM final) to initiate the reaction. Assays were performed in triplicate at 37 °C for 4 min with time points taken at 1, 2, 3, and 4 min. Each time aliquot was treated as described for the HPLC-FLD method to detect the formation of L-tyrosine. Assay controls included the same concentrations as the activity assay sample: (1) Orf13 only, (2) Orf13 and L-phenylalanine, (3) L-phenylalanine, (4) L-phenylalanine with hydrogen peroxide, (5) L-tyrosine, and (6) 100 μM L-tyrosine with hydrogen peroxide. All controls were run in triplicate the same day as the assay samples containing Orf13, L-phenylalanine, and hydrogen peroxide and underwent the same method work-up described. Assays using the substrate analogues DL-*m*-tyrosine, tyramine, 3-(4-hydroxylphenyl)propanoic acid, and *p*-cresol were monitored by the L-DOPA colorimetric assay for their respective catechol products; L-DOPA, dopamine, 3-(3,4-hydroxyphenyl)propanoic acid, and 4-methylcatechol. Orf13 (1.5 μM) was incubated with L-tyrosine (5 mM final) or substrate analogue (5 mM final) for 5 min at 37 °C in 100 mM sodium phosphate (pH 8.0), followed by addition of hydrogen peroxide (500 μM final) to initiate the reaction. At 2 min, a time aliquot from each substrate analogue reaction was taken, underwent the same colorimetric work-up as described, and was scanned using a Varian UV−vis Cary100 spectrophotometer for the formation of the catechol−nitrite complex. For assays assessing the relative specific activity for substrate selectivity, Orf13 (1.5 μM) was incubated with L-tyrosine (5 mM final) or substrate analogue (5 mM final) for 5 min at room temperature in 100 mM sodium phosphate (pH 8.0), followed by addition of hydrogen peroxide (250 μM final) to initiate the reaction. Assays were performed in triplicate with each substrate at room temperature for 11 min with time aliquots taken at 1, 3, 6, and 11 min. Standard curves of the respective catechol products from 1 to 100 μM were prepared the same day for each set of assays. These substrate analogues and catechol products were quantified spectrophotometrically at $\varepsilon_{275\ nm}$ = 1.4 mM^{-1} cm^{-1} and $\varepsilon_{280\ nm}$ = 2.63 mM^{-1} cm^{-1}, respectively. Assay controls with a blank solution without Orf13 were used to correct for background. Orf13 background control assays were carried out with the same concentration of enzyme in the absence of substrates. No enzyme background at 500 nm was observed with 1.5 μM Orf13 or less. All controls were run in triplicate and in parallel with assay samples and underwent the same colorimetric work-up described above.

RESULTS AND DISCUSSION

Expression and Purification of Native Orf13 in BL21(DE3) *E. coli*. Cell pellets after overexpression of Orf13 are red in color, and the color of the expression media becomes dark brown or black when expression is continued for more than 8 h. The red cell color was the first indication of a cofactor likely bound to Orf13, while production of the black pigment suggested the enzyme to be active since this has been observed for the oxidative polymerization of L-DOPA.[28] Non-fusion-tagged Orf13 showed affinity for Ni-Sepharose resin and was utilized for purification. Auto-oxidative degradation of Orf13, observed by SDS-PAGE (Figure S2C) by the appearance of a band of MW consistent with a covalent dimer, correlated with a distinct color change of the enzyme from dark red to brownish-yellow and occurred at purification steps that did not contain excess DTT (50 mM) or ascorbate (25 mM) or had removed imidazole from the buffer during gel filtration. The formation of an apparent covalent dimer and spectral changes of the heme seem to indicate that oxidative damage occurs both at an amino acid residue and at the heme. Protection of Orf13 by including either DTT (50 mM), ascorbate (25 mM), or imidazole (10 mM) during gel filtration is achieved by reduction of the heme or by scavenging radicals. Pure and stable Orf13 exists as a monomer in solution with an experimentally observed molecular weight of 37.9 kDa consistent with the predicted monomeric weight of 33.6 kDa.

Heme b Is Bound to Orf13. Characteristic absorbance bands of a heme moiety were observed in a UV−vis absorption spectrum of purified Orf13 (Figure 2). The Soret band at 408 nm indicated a ferric heme iron in a pentacoordinate state based on the presence of a Q-band at 630 nm. Heme b was identified as the heme moiety noncovalently bound to Orf13 by coelution with standard heme b by HPLC (Figure 3). The HPLC peak at 42 min from the supernatant of denatured Orf13 was confirmed as heme b with subsequent ESI-MS/MS analysis (Figure S4). No other organic cofactors were identified with Orf13, and no other metals, other than iron originating from heme b, were found by ICP-MS. This information excludes classification of Orf13 as any of the non-heme dependent monophenol monooxygenases previously mentioned, in particular, the non-heme iron pterin or α-KG dependent enzymes and the copper dependent tyrosinases that catalyze the *ortho*-hydroxylation of L-tyrosine to L-DOPA.[15,16]

Stoichiometry of Heme b in Orf13. A wide range of heme b occupancy from 10% to 100% was observed with Orf13 purified under conditions protecting the enzyme from

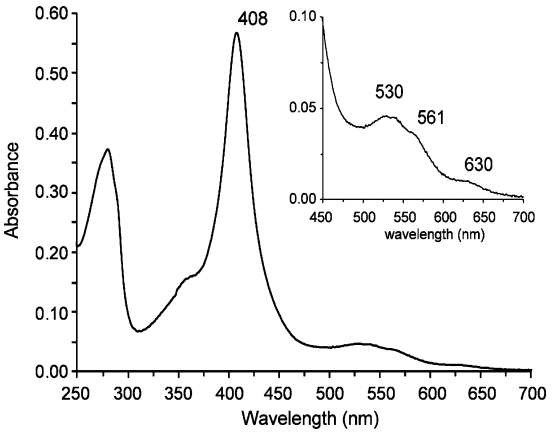

Figure 2. UV−vis absorption spectrum of purified Orf13 (100% heme b occupancy) in 20 mM Tris-HCl (pH 8.0), 10 mM imidazole, and 10% glycerol. The Soret band of heme b is observed at 408 nm and Q-bands at 530, 561, and 630 nm (inset).

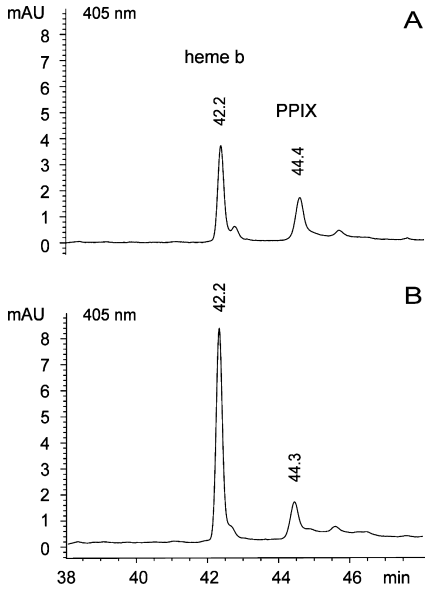

Figure 3. HPLC chromatograms for porphyrin detection: (A) supernatant of denatured Orf13 sample; (B) co-injection of the sample shown in (A) with heme b standard.

degradation. Orf13 with 100% heme b occupancy has a RZ value of 1.8 based on the ratio of the heme absorbance at 408 nm to protein absorbance at 280 nm. (Note: 100% heme b occupancy is defined as 1 heme b moiety per monomer of enzyme.) We determined that Orf13 is also occupied by PPIX and the amount of PPIX bound to Orf13 made up the occupancy difference when substoichiometric amounts of heme b were measured in purified enzyme (i.e., 75% heme b and 25% PPIX). The presence of a second porphyrin species bound to Orf13 other than heme b was evident by the appearance of two distinct Soret band species at 406 and 431 nm in dithionite reduced enzyme (Figure S5). The Soret band species at 406 nm is PPIX, which remains unaffected by dithionite as it lacks an iron center. The presence of PPIX bound to Orf13 was further confirmed after coinjection of PPIX with Orf13 showed an increase of the peak observed at 44 min (coinjection data not shown, refer to Figure 3) and subsequent ESI-MS/MS analysis (Figure S6). The amount of PPIX bound to Orf13 was determined by a calibration curve using HPLC and spectrophotometrically quantified PPIX ($\varepsilon_{408\ nm}$ = 262 mM^{-1} cm^{-1} in 2.7 M HCl[29]) from which the stoichiometry was calculated by the molar ratio of PPIX and Orf13. This is the first reported case where a heme containing enzyme has been found to be fully occupied with a heterogeneous mixture of heme b and PPIX. Dissociation constants of heme b for enzymes utilizing the heme moiety in different capacities show a range in heme binding affinities: myoglobin for oxygen transport (1.3×10^{-14} M),[30] bovine serum albumin for transport (4.6×10^{-9} M),[31] *pa*-HO, a heme oxygenase, for heme degradation (0.6×10^{-6} M) and PhuS involved in heme binding, trafficking, and transfer (0.2×10^{-6} M).[32] The dissociation constant of PPIX for ferrochelatase (1.5×10^{-6} M)[33] has similar binding affinity as *pa*-HO and PhuS have for heme b. Heme b and PPIX are tightly bound to Orf13 as there is no exchange or loss during dialysis unless the enzyme is denatured with 6 M guanidinium hydrochloride or 2% SDS to remove either species. The occupancy ranges of heme b and PPIX with Orf13 may indicate this enzyme to have similar binding affinities for both porphyrin moieties. The lack of *in vivo* binding discrimination between heme b and PPIX may also suggest stronger binding interactions with protein residues and substituents of porphyrin ring (i.e., the propanoic acid or vinyl groups) than the axial residues coordinating the heme iron.

The extensive variability in heme b occupancy for Orf13 was observed in expression batches from the same seed culture, prepared in the same liquid media, and grown and expressed on the same shaker using identical flasks. Heme dependent enzymes obtained from *E. coli* expression systems that require a noncovalently bound heme are predominantly an apo form with partial heme occupancy without the presence of PPIX.[34−36] Complete heme occupancy can be readily achieved by addition of heme to the enzyme by titration without the need for protein denaturation and refolding. *In vitro* titration of heme b to purified Orf13 did not exchange the bound PPIX, and the enzyme remained fully occupied with a heterogeneous mixture of both porphyrin species. Attempts to obtain an apo form of Orf13 for *in vitro* heme titration was also unsuccessful since the enzyme failed to express when 1,10-phenanthroline, a metal chelating agent, was added to the growth medium. In an effort to increase and control the *in vivo* incorporation of heme b in Orf13, δ-aminolevulinic acid (δ-ALA, a heme biosynthetic precursor[37]), exogenous non-heme iron with or without δ-ALA, or exogenous hemin was added to the medium for expression in BL21(DE3) *E. coli*. This strategy was ineffective as similar results in heme b occupancy (30−100%) were observed compared to Orf13 expression without any additives. It was also determined that the range in heme b and PPIX occupancies with Orf13 is independent of the purification method. Purification of Orf13 by anionic exchange (Q-Sepharose) in the presence of excess DTT (50 mM) to protect Orf13 from auto-oxidative degradation showed the same variable heme b occupancies as the metal affinity method (Ni-Sepharose). This confirmed that heme b bound to Orf13 was not compromised, lost, or competed out due to the enzyme's ability to intrinsically bind to Ni-Sepharose.

An alternative *E. coli* expression system for *in vivo* incorporation of heme b in Orf13 was tried using RP523 *E. coli* with exogenous hemin. RP523 is a porphyrin permeable strain of *E. coli* with a mutation in the *hemB* gene of the heme biosynthetic pathway that disrupts the normal biosynthesis of heme b causing the cells to be dependent on the uptake of exogenous heme b for survival.[38] This expression system has

Table 1. Steady-State Kinetic Parameters for L-Tyrosine Hydroxylation by Orf13[a]

variable substrate	fixed substrate	K_m[b] (mM)	k_{cat} (s^{-1})	k_{cat}/K_m (M^{-1} s^{-1})
L-tyrosine	H_2O_2	0.45 ± 0.04	0.576 ± 0.005	(1.2 ± 0.1) × 10^3
H_2O_2	L-tyrosine	1.0 ± 0.3	1.5 ± 0.3	(1.5 ± 0.2) × 10^3

[a]Assays were performed at 37 °C with 0.3−1 μM Orf13 (75% heme b occupancy) in 100 mM sodium phosphate (pH 8.0). L-DOPA formation was measured using the L-DOPA colorimetric assay. [b]These values are apparent K_m constants at saturating concentrations of the other substrate. Mean and standard error are reported.

been established for substituting nitric oxide synthase (NOX), a heme dependent enzyme, with different metalloporphyrins.[19,39] The advantage in utilizing this system for Orf13 expression is that these cells lack the ability to synthesize porphyrin and are only viable in the presence of heme b, thus eliminating the presence of PPIX with Orf13. RP523 *E. coli* cells expressing Orf13 using the pCW/*orf13* construct were red in color as observed with Orf13 expression in BL21(DE3) *E. coli*. However, it was difficult to obtain stable Orf13 using the developed purification methods previously described. Severe degradation of Orf13 was evident with the Ni-Sepharose method in the presence of imidazole. Orf13 eluted as a brownish-yellow enzyme and showed auto-oxidative degradation by SDS-PAGE with a predominant protein band at double the monomeric weight of Orf13 as previously observed in purifications from BL21(DE3) *E. coli* without oxidative protection (Figure S2C). Repeating the Ni-Sepharose purification under anaerobic conditions in a glovebox prevented dimerization of Orf13, and the enzyme retained its red color. The visible absorption spectrum of heme b bound to Orf13 was similar to Orf13 purified from BL21(DE3) *E. coli* (refer to Figure 2). However, the overall yield and purity were very poor. Purification by the Q-Sepharose method with excess DTT (50 mM) prevented covalent dimerization and improved the purity of the protein sample. However, Orf13 eluted as a bright yellow enzyme with an unusual visible absorption spectrum of the heme displaying a broad Soret band at 420 nm without distinguishable Q-bands. In addition, the heme species bound to Orf13 could not be reduced by dithionite to assess its heme b stoichiometry by the pyridine hemochromagen method. Overall, the feasibility in obtaining sufficient amounts of highly pure and stable Orf13 fully occupied with heme b from RP523 *E. coli* was unsuccessful and proved more challenging than the purification of Orf13 expressed in BL21(DE3) *E. coli*.

Catalytic Assessment of Heme b for L-Tyrosine Hydroxylation. Orf13 was not expected to be a heme dependent cytochrome 450-like enzyme since there are no conserved cysteine or methionine residues (Figure S1). This was confirmed when DTT or dithionite reduced Orf13 in the presence of L-tyrosine did not produce L-DOPA. Production of L-DOPA was observed when hydrogen peroxide was added to Orf13 in the presence of L-tyrosine (Figure S7). This implicated the catalytic requirement of heme b. A modified discontinuous assay for spectrophotometric detection of L-DOPA in a L-DOPA−nitrite colorimetric complex[25,26] was utilized to measure the specific activity and steady-state kinetics of Orf13 (Table 1) due to the limited sensitivity of the HPLC-FLD analysis. The specific activity of Orf13 for the hydrogen peroxide dependent reaction correlated with the stoichiometry of heme b where maximal turnover of ferric heme Orf13 (100% heme b) was 32 ± 2 min^{-1} compared to 21 ± 1 min^{-1} with ferric heme Orf13 (48% heme b). The specific activity was also dependent on the heme iron oxidation state where ferric heme Orf13 (48% heme b) had greater catalytic activity (21 ± 1 min^{-1}) than Orf13 with ferrous heme in the presence of 50 mM DTT (9 ± 1 min^{-1}). This is in agreement with a catalytic starting state of ferric heme iron for heme peroxidases.[40] These results established heme b as the cofactor required for catalysis, classifying Orf13 as a heme dependent peroxidase catalyzing the *ortho*-hydroxylation of L-tyrosine to L-DOPA. The steady-state rate constants for L-tyrosine and hydrogen peroxide were determined using the L-DOPA colorimetric assay and the preincubation condition of Orf13 with L-tyrosine prior to reaction initiation by addition of hydrogen peroxide (Table 1; Figure S8 for Michaelis−Menten curves). The steady-state kinetic parameters for L-tyrosine hydroxylation by Orf13 fit to the Michaelis−Menten model are within the range of values reported for other heme peroxidases,[41] and the catalytic efficiencies for both substrates are similar.

Tyrosine hydroxylation to L-DOPA by Orf13 is also observed in the presence of L-ascorbate or DHFA (Figure S9). The ascorbate and DHFA dependent reactions require molecular oxygen and have similar k_{obs} that are 48- and 58-fold less than the k_{obs} of the hydrogen peroxide dependent reaction, respectively (Table 2). Aromatic hydroxylation by the DHFA dependent reaction was abolished in the presence of SOD and was not observed with catalase, while the ascorbate dependent

Table 2. Reaction Dependence Behavior of Orf13 for L-Tyrosine Hydroxylation

assay condition[a,b]	k_{obs} (min^{-1})[c]	rel percentage[d]
Orf13	none	0
Orf13 + H_2O_2	34 ± 4	100
Orf13 + H_2O_2 -O_2	33 ± 3	98
Orf13 + H_2O_2 + catalase (75 μg/mL)	1.6 ± 0.2	5
Orf13 + H_2O_2 + SOD (100 μg/mL)	26.5 ± 0.6	78
Orf13 + AscA	0.58 ± 0.01	1.7
Orf13 + AscA - O_2	none	0
Orf13 + AscA + catalase (75 μg/mL)	0.15 ± 0.01	0.5
Orf13 + AscA + SOD (100 μg/mL)	0.59 ± 0.1	1.7
Orf13 + DHFA	0.69 ± 0.06	2
Orf13 + DHFA - O_2	none	0
Orf13 + DHFA + catalase (75 μg/mL)	none	0
Orf13 + DHFA + SOD (100 μg/mL)	none	0

[a]Abbreviations: tyrosine hydroxylase (Orf13), hydrogen peroxide (H_2O_2), molecular oxygen (O_2), L-ascorbate (AscA), dihydroxyfumaric acid (DHFA), superoxide dismutase (SOD). [b]Final assay concentrations: 0.5 or 2.5 μM Orf13 (75% heme b occupancy), 5 mM L-tyrosine in 100 mM sodium phosphate (pH 8.0) at 37 °C; 25 mM AscA, 2 mM DHFA, or 500 μM H_2O_2 as indicated by assay condition. L-DOPA detected by L-DOPA colorimetric assay for H_2O_2 dependent reactions and by HPLC-FLD for AscA and DHFA dependent reactions. [c]Mean and standard deviation reported for k_{obs}. [d]Relative percentage is based on Orf13 + H_2O_2 condition where maximal turnover is observed.

dx.doi.org/10.1021/bi201148a | *Biochemistry* 2011, 50, 8926−8936

reaction was not affected by SOD and decreased 4-fold in the presence of catalase. Interestingly, hydroxylation of phenols has been reported for horseradish peroxidase (HRP) in the presence of DHFA as an oxygen transfer reaction similar to cytochrome P450 enzymes.[42,43] The peroxygenase activity of HRP is promoted by nonenzymatic production of superoxide by DHFA and molecular oxygen, which then causes the formation of compound III, an oxyferrous heme-iron state, when superoxide binds to the heme. Hydroxylation of phenol only occurs when substrate and additional reducing equivalents of DHFA are present with HRP−compound III.[42] Hydroxylation of L-tyrosine to L-DOPA by Orf13 in the presence of DHFA is in agreement with the HRP peroxygenase activity for aromatic hydroxylation. Although molecular oxygen dependent hydroxylation of L-tyrosine by Orf13 in the presence of ascorbate or DHFA is observed, it does not appear to be the primary catalytic pathway for L-tyrosine hydroxylation since turnover is enhanced 48- and 58-fold, respectively, when hydrogen peroxide is provided as a substrate for the hydroxylation reaction even in the absence of molecular oxygen under anaerobic conditions (Table 2).

HRP and other heme peroxidases such as myeloperoxidase and chloroperoxidase are known to catalyze dimerization of aromatic substrates in the presence of hydrogen peroxide by way of the classical two sequential one-electron transfer mechanism.[27,44,45] However, hydroxylation of aromatic amino acids in the presence of hydrogen peroxide by heme peroxidases has not been reported.[42] These results emphasize the novelty of Orf13 for its ability to use hydrogen peroxide for aromatic hydroxylation of L-tyrosine. A possible mechanism for this reaction may share the initial steps of the classic heme peroxidase catalytic cycle up to the formation of compound I (Scheme 1).[27,44,45] Compound I is also an intermediate in the

Scheme 1. Proposed Mechanism for *Ortho*-hydroxylation of L-Tyrosine by Orf13

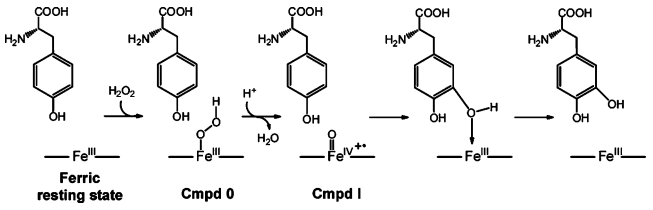

hydroxylation reactions catalyzed by P450 enzymes for the oxygen dependent reaction and the peroxide shunt pathway.[17,46] It has also been proposed in the hydrogen peroxide dependent hydroxylation reactions of heme−thiolate peroxygenases.[17,47] As these peroxygenases represent heme−thiolate enzymes functioning more like heme peroxidases in their substrate specificity for hydrogen peroxide,[17,47] Orf13 may represent the first heme−histidyl enzyme and mechanistic bridge between the heme peroxidases and the P450 enzymes. Therefore, subsequent steps after formation of compound I may be reminiscent of the electron rebound mechanism proposed by Groves for P450 enzymes (Scheme 1).[46,48] Formation of the product complex with the oxygen coordinated to the iron(III) center may proceed through a hydroxyl iron(IV) substrate radical complex obtained by hydrogen abstraction by compound I from the substrate.[48] Alternatively, this substrate radical could react with a second substrate radical similarly produced to yield the dimeric product characteristic of peroxidase reactions.[27,40] The fate of the reaction either toward hydroxylation or dimerization depends on the reactivity of the compound I complex, which is controlled by steric and electronic interactions in the active site.[49,50] These interactions may significantly reduce the lifetime of this radical intermediate preventing dimerization and/or may stabilize the hydroxylation transition state.

Sequence Analysis of Orf13 as a Heme Peroxidase. Spectroscopic data supporting Orf13 as a heme peroxidase are evident by a Soret band position at 421 nm in a reduced-CO spectrum of Orf13 (Figure 4A) and a low-temperature electron paramagnetic resonance spectrum of ferric heme Orf13 showing a predominant high spin heme iron with a *g*-value centered at 5.8 (Figure 4B). This spectroscopic data with the comparative analysis of the highly conserved residues in Orf13 (Figure S1) to other heme peroxidases suggests a histidyl-ligated heme iron. However, Orf13 and its homologues were not initially identified as heme dependent peroxidases by BLAST (blastp) analysis nor by the PeroxiBase database[51] (http://peroxidase.isb-sib.ch/). Reassessment of the conserved residues in the multiple sequence alignment of Orf13 and homologues reveals some similarity to the conserved distal site motif $RX_2F(W)H$ characteristic of class I, II, and III peroxidases represented by ascorbate peroxidase, *Arthromyces ramosus* peroxidase, and HRP, respectively. These heme peroxidases have a proximal histidine residue coordinating the heme iron as the fifth ligand between 120 and 138 residues away from the conserved distal histidine.[52−55] In Orf13, a highly conserved region containing $R^{71}W^{72}X_3H^{76}$ has the same conserved residues as the distal site $RX_2F(W)H$ motif of class I, II, and III peroxidases. The similarity in these motifs between unrelated enzymes suggests the evolutionary adaptation for the utilization of hydrogen peroxide for oxidative reaction by heme dependent enzymes. However, residue spacing is different between W72 and H76 than the R and F/W, and the two highly conserved histidine residues (H140 and H184), one of which may act as the proximal heme-iron ligand, are closer in sequence to H76 of the potential distal site by 63 and 107 residues, respectively. These differences in sequence spacing within the potential distal site motif and the proximal histidine may explain why Orf13 was not recognized as a heme peroxidase and might be required for the different reactivity of Orf13 compared to class I, II, and III peroxidases, revealing the existence of a new class of bacterial heme peroxidases.

Evaluation of Substrate Order for Catalysis and Inactivation by Hydrogen Peroxide. Heme peroxidases typically bind hydrogen peroxide first, although the heme iron can become trapped in a nonproductive oxyferrous state (compound III) during the catalytic cycle.[40] Characteristic bands for compound III in HRP include a Soret band at 417 nm and Q-bands at 544 and 580 nm.[56] For Orf13, reversed substrate order of addition is necessary for catalysis with preincubation with L-tyrosine prior to the addition of hydrogen peroxide (Figure S10). No turnover is observed if hydrogen peroxide is incubated with Orf13 before the addition of L-tyrosine. UV−vis absorption scans of Orf13 were taken before and after addition of hydrogen peroxide in the absence of L-tyrosine to investigate whether the lack of catalysis by the hydrogen peroxide Orf13 complex is due to formation of compound III (Figure 5A). The spectrum measured in the presence of hydrogen peroxide shows a significant decrease in the Soret band intensity and disappearance of the Q bands at 503 and 630 nm that is unlike the characteristic spectrum of

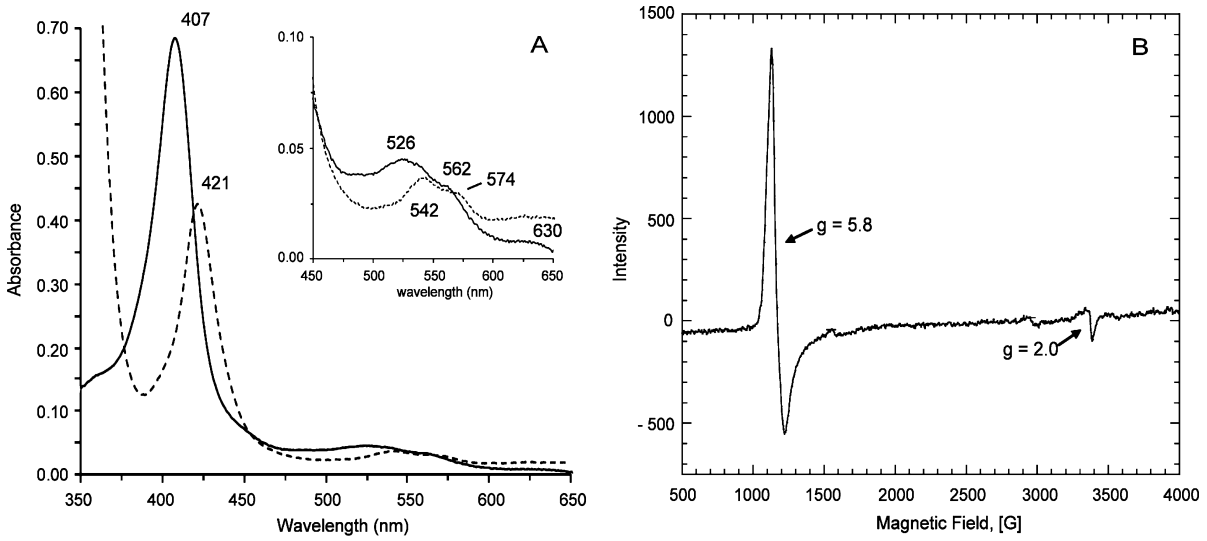

Figure 4. (A) UV−vis absorption spectrum of ferric heme Orf13 (solid line) and ferrous CO heme (g) Orf13 (dashed line) with 100% heme b occupancy in 20 mM Tris-HCl (pH 8.0), 10 mM imidazole and 10% glycerol. (B) X-band EPR spectrum of ferric-heme Orf13 at 15 K. Experimental conditions: 90 μM Orf13 with 50% heme b occupancy (45 μM heme b) in 10 mM sodium phosphate (pH 8.0) and 50% glycerol; frequency, 9.478 GHz; microwave power, 201 μW; modulation frequency, 100 kHz; modulation amplitude, 10.0 G; receiver gain, 5×10^3.

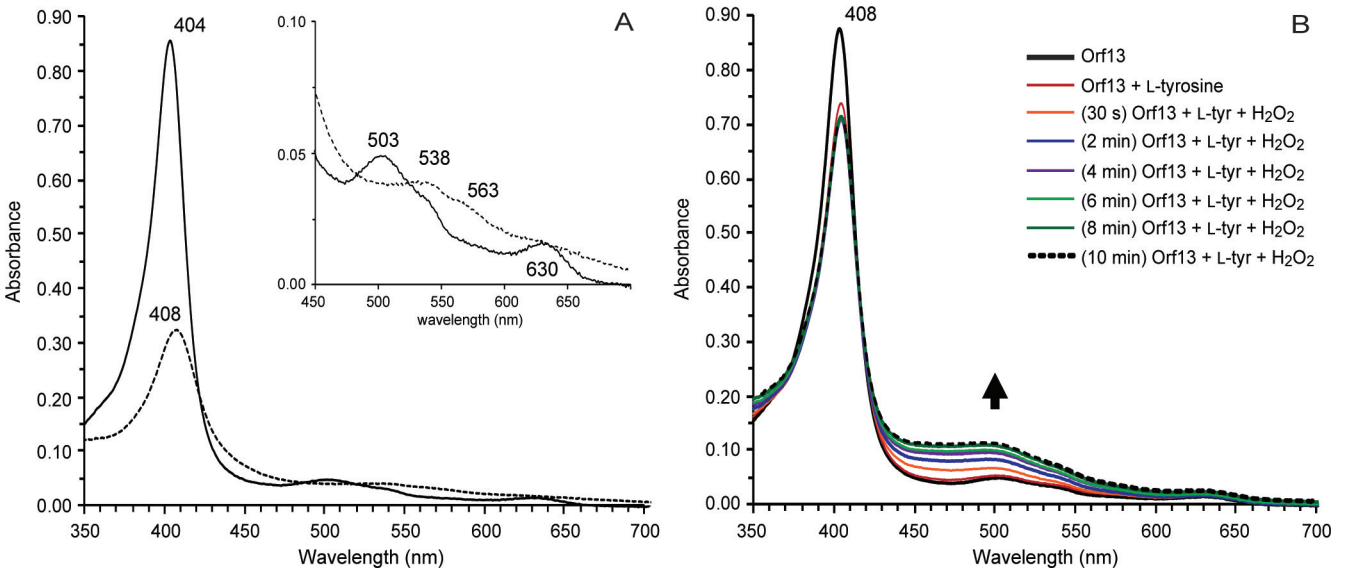

Figure 5. UV−vis absorption spectra of Orf13 (100% heme b). (A) Orf13 (4 μM) in the absence (solid line) and presence (dashed line) of 500 μM hydrogen peroxide in 100 mM sodium phosphate (pH 8.0) at room temperature. (B) Orf13 with L-tyrosine followed by the addition of hydrogen peroxide. Final experimental conditions: 4 μM Orf13, 5 mM L-tyrosine, 500 μM hydrogen peroxide in 100 mM sodium phosphate (pH 8.0) at room temperature. The sample was scanned at 2 min intervals for 10 min after the addition of hydrogen peroxide.

HRP−compound III. However, the formation of compound III may be transient for Orf13 even though this heme iron state has been shown to be stable in HRP for at least 5 min.[56] This may suggest a different hydrogen peroxide inactivation mechanism for Orf13.

No changes in the heme spectrum were observed by addition of L-tyrosine to Orf13. This may indicate that the role of L-tyrosine as the first substrate added is simply to protect Orf13 from hydrogen peroxide inactivation and does not affect the coordination of the heme iron as shown by the retention of the 630 nm Q-band (Figure 5B). Interaction of L-tyrosine at the heme edge is consistent as there are no changes in the heme spectrum and is evident in heme spectra during catalysis after the addition of hydrogen peroxide to Orf13 preincubated with L-tyrosine (Figure 5B). During catalysis the absorbance intensity from 450 to 600 nm, most notable in the Q-band at 503 nm, increased over time up to 6 min, after which no more changes were observed. The pattern of absorbance change at 503 nm is similar to what is observed for L-DOPA production by the colorimetric assay when Orf13 is preincubated with L-tyrosine and the reaction initiated with hydrogen peroxide (Figure S10). The increase in the 503 nm Q-band is similar to a dehaloperoxidase bound complex with 2,4-dichloroquinone product[57] and could therefore be attributed to an Orf13 bound complex with L-DOPA.

Substrate Specificity for the Hydrogen Peroxide Dependent Aromatic Hydroxylation Reaction by Orf13. Heme peroxidases are promiscuous enzymes capable

dx.doi.org/10.1021/bi201148a | Biochemistry 2011, 50, 8926–8936

of oxidizing a wide assortment of aromatic substrates. Their lack of substrate specificity has been attributed to a larger active site that can accommodate various substrates, as well as the presence of additional substrate binding locations in the vicinity of the exposed heme edges where the reaction can also occur.[58] The substrate analogues L-phenylalanine, DL-*m*-tyrosine, tyramine, 3-(4-hydroxyphenyl)propanoic acid, and *p*-cresol were selected to test the substrate specificity of Orf13 (Figure S11) as well as to evaluate the requirement of chemical substituents on the aromatic ring in order for the hydroxylation reaction to occur. The *para*-substituted phenols (tyramine, 3-(4-hydroxyphenyl)propanoic acid, and *p*-cresol) were converted by Orf13 in the presence of hydrogen peroxide to their respective catechol products, which were detected as colorimetric catechol−nitrite complexes using the L-DOPA colorimetric assay (Figure S12). Comparison of the relative specific activity of these substrate analogues to L-tyrosine was unsuccessful as formation of the product analogues plateaued after the first minute of turnover, while L-DOPA formation from L-tyrosine remained linear up to 6 min (Figure S13). Orf13 is more susceptible to inactivation by hydrogen peroxide in the presence of these substrate analogues than with L-tyrosine. No increase in catechol product formation was detected when L-tyrosine was added to the *p*-cresol reaction after 1 min, confirming the inactivation of Orf13 (data not shown). No L-phenylalanine conversion to L-tyrosine was observed using an HPLC-FLD method to detect L-tyrosine, and no L-DOPA formation was observed using the L-DOPA colorimetric assay when DL-*m*-tyrosine was provided as a substrate. These results show that the hydroxyl group at the *para* position of the aromatic ring is necessary for hydroxylation since conversion of L-tyrosine, tyramine, 3-(4-hydroxyphenyl)-propanoic acid, and *p*-cresol to their respective catechol products is observed. Moreover, *ortho*-hydroxylation by Orf13 seems to be specific for L-tyrosine as the only substrate that protects from hydrogen peroxide inactivation.

In conclusion, we have successfully purified and confirmed the putative function of Orf13 from the anthramycin biosynthetic pathway as a tyrosine hydroxylase. The sequence of Orf13 is not similar to any known characterized proteins, nor does it contain conserved domains or motifs characteristic of enzymes performing hydroxylation reactions. We have provided spectroscopic and kinetic evidence that classifies Orf13 as a heme dependent peroxidase. Similar to heme−histidyl peroxidases, Orf13 displays a secondary hydroxylation activity of aromatic substrates in the presence of molecular oxygen and L-ascorbate or DHFA. However, unlike these heme peroxidases this enzyme catalyzes hydrogen peroxide dependent *ortho*-hydroxylation instead of dimerization by radical coupling, and the substrate order of addition is reversed with a required preincubation with L-tyrosine for activity. Orf13 can hydroxylate other *para*-substituted phenols but is inactivated by hydrogen peroxide much more readily than when L-tyrosine is the substrate. This implicates a catalytic mechanism requiring the *para*-phenol substituent for hydroxylation as no turnover for L-phenylalanine or DL-*m*-tyrosine was observed as well as demonstrates the substrate selectivity for L-tyrosine. Therefore, we propose that Orf13 represents a new class of heme−histidyl ligated hydrogen peroxide dependent hydroxylases. In addition, Orf13 is the first identified heme peroxidase specific for L-tyrosine and is the first identified bacterial tyrosine hydroxylase.

■ ASSOCIATED CONTENT

Ⓢ Supporting Information

Additional supplementary figures and data including the multiple sequence analysis, purification gels, UV−vis and mass spectrometry spectra, kinetic data, and substrate specificity results described in the text. This material is available free of charge via the Internet at http://pubs.acs.org.

■ AUTHOR INFORMATION

Corresponding Author

*Tel: 1 (301) 405-3949. Fax: 1 (301) 314-9121. E-mail: bgerrata@umd.edu.

Funding

This work was supported by NIH Grant GM084473 (B.G).

■ ACKNOWLEDGMENTS

We thank Dr. Charles Long, Dr. Amanda J. McGown, and Dr. David P. Goldberg for their assistance with the low-temperature EPR experiment; Dr. Michael A. Marletta for the generous gifts of the pCW vector and RP523 *E. coli* strain; Dr. Zvi Kelman for use of the Superdex200 gel filtration system to determine the quaternary structure of Orf13 in solution; and Dr. Steven E. Rokita for helpful discussions.

■ ABBREVIATIONS

PBD, pyrrolo[1,4]benzodiazepine; ICP-MS, inductively coupled plasma mass spectrometry; HPLC-FLD, high performance liquid chromatography fluorescence detection; ESI-MS/MS, electrospray ionization mass spectrometry with tandem mass spectrometry; PPIX, protoporphyrin IX; *δ*-ALA, *δ*-aminolevulinic acid; DTT, dithiothreitol; SOD, superoxide dismutase; DHFA, dihydroxyfumaric acid; HRP, horseradish peroxidase.

■ REFERENCES

(1) Gerratana, B. (2011) Biosynthesis, synthesis, and biological activities of pyrrolobenzodiazepines. *Med. Res. Rev.*, DOI: 10.1002/med.20212.

(2) Spízek, J., and Rezanka, T. (2004) Lincomycin, clindamycin and their applications. *Appl. Microbiol. Biotechnol. 64*, 455−464.

(3) Rössner, E., Zeeck, A., and König, W. A. (1990) Elucidation of the Structure of Hormaomycin. *Angew. Chem., Int. Ed. Engl. 29*, 64−65.

(4) Hurley, L. H., Lasswell, W. L., Ostrander, J. M., and Parry, R. (1979) Pyrrolo[1,4]benzodiazepine antibiotics. Biosynthetic conversion of tyrosine to the C2- and C3-proline moieties of anthramycin, tomaymycin, and sibiromycin. *Biochemistry 18*, 4230−4237.

(5) Brahme, N. M., Gonzalez, J. E., Rolls, J. P., Hessler, E. J., Mizsak, S., and Hurley, L. H. (1984) Biosynthesis of the lincomycins. 1. Studies using stable isotopes on the biosynthesis of the propyl- and ethyl-L-hygric acid moieties of lincomycins A and B. *J. Am. Chem. Soc. 106*, 7873−7878.

(6) Höfer, I., Crüsemann, M., Radzom, M., Geers, B., Flachshaar, D., Cai, X., Zeeck, A., and Piel, J. (2011) Insights into the Biosynthesis of Hormaomycin, An Exceptionally Complex Bacterial Signaling Metabolite. *Chem. Biol. 18*, 381−391.

(7) Peschke, U., Schmidt, H., Zhang, H.-Z., and Piepersberg, W. (1995) Molecular characterization of the lincomycin-production gene cluster of *Streptomyces lincolnensis* 78−11. *Mol. Microbiol. 16*, 1137−1156.

(8) Novotna, J., Honzatko, A., Bednar, P., Kopecky, J., Janata, J., and Spizek, J. (2004) L-3,4-Dihydroxyphenyl alanine-extradiol cleavage is followed by intramolecular cyclization in lincomycin biosynthesis. *Eur. J. Biochem. 271*, 3678−3683.

(9) Neusser, D., Schmidt, H., Spizek, J., Novotna, J., U., P., Kaschabeck, S., Tichy, P., and Piepersberg, W. (1998) The genes lmbB1 and lmbB2 of *Streptomyces lincolnensis* encode enzymes involved in the conversion of L-tyrosine to propylproline during the biosynthesis of the antibiotic lincomycin A. *Arch. Microbiol. 169*, 322–332.
(10) Hu, Y., Phelan, V., Ntai, I., Farnet, C. M., Zazopoulos, E., and Bachmann, B. O. (2007) Benzodiazepine Biosynthesis in *Streptomyces refuineus*. *Chem. Biol. 14*, 691–701.
(11) Li, W., Chou, S., Khullar, A., and Gerratana, B. (2009) Cloning and Characterization of the Biosynthetic Gene Cluster of Tomaymycin, an SJG-136 monomeric analog. *Appl. Environ. Microbiol. 75*, 2958–2963.
(12) Li, W., Khullar, A., Chou, S., Sacramo, A., and Gerratana, B. (2009) Biosynthesis of Sibiromycin, a potent antitumor antibiotic. *Appl. Environ. Microbiol. 75*, 2869–2878.
(13) Sono, M., Roach, M. P., Coulter, E. D., and Dawson, J. H. (1996) Heme-Containing Oxygenases. *Chem. Rev. 96*, 2841–2888.
(14) Leahy, J. G., Batchelor, P. J., and Morcomb, S. M. (2003) Evolution of the soluble diiron monooxygenases. *FEMS. Microbiol. Rev. 27*, 449–479.
(15) Fitzpatrick, P. F. (2003) Mechanism of Aromatic Amino Acid Hydroxylation. *Biochemistry 42*, 14083–14091.
(16) Rosenzweig, A. C., and Sazinsky, M. H. (2006) Structural insights into dioxygen-activating copper enzymes. *Curr. Opin. Struct. Biol. 16*, 729.
(17) Ullrich, R., and Hofrichter, M. (2007) Enzymatic hydroxylation of aromatic compounds. *Cell. Mol. Life. Sci. 64*, 271.
(18) Koehntop, K. D., Emerson, J. P., and Que, L. (2005) The 2-His-1-carboxylate facial triad: a versatile platform for dioxygen activation by mononuclear non-heme iron(II) enzymes. *J. Biol. Inorg. Chem. 10*, 87–93.
(19) Woodward, J. J., Martin, N. I., and Marletta, M. A. (2007) An *Escherichia coli* expression-based method for heme substitution. *Nature Methods 4*, 43–45.
(20) Berry, E. A., and Trumpower, B. L. (1987) Simultaneous determination of hemes *a*, *b*, and *c* from pyridine hemochrome spectra. *Anal. Biochem. 161*, 1–15.
(21) Olsovská, J., Novotná, J., Flieger, M., and Spízek, J. (2007) Assay of tyrosine hydroxylase based on high-performance liquid chromatography separation and quantification of L-dopa and L-tyrosine. *Biomed. Chromatogr. 21*, 1252–1258.
(22) Edelhoch, H. (1962) The Properties of Thyroglobulin. *J. Biol. Chem. 237*, 2778–2787.
(23) *The Merck Index*, 13th ed., entry # 5485.
(24) Hiner, A. N., Rodriguez-Lopez, J. N., Arnao, M. B., Lloyd Raven, E., Garcia-Canovas, F., and Acosta, M. (2000) Kinetic study of the inactivation of ascorbate peroxidase by hydrogen peroxide. *Biochem. J. 348*, 321–328.
(25) Arnow, L. E. (1937) Colormetric Determination of the Components of 3,4-dihydroxyphenylalanine-tyrosine Mixtures. *J. Biol. Chem. 118*, 531–537.
(26) Fitzpatrick, P. F. (1991) Steady-state kinetic mechanism of rat tyrosine hydroxylase. *Biochemistry 30*, 3658–3662.
(27) Marquez, L. A., and Dunford, H. B. (1995) Kinetics of Oxidation of Tyrosine and Dityrosine by Myeloperoxidase Compounds I and II. *J. Biol. Chem. 270*, 30434–30440.
(28) Morris, F. (1950) Non-Enzymatic Oxidation of Tyrosine and Dopa. *Proc. Natl. Acad. Sci. U. S. A. 36*, 606–611.
(29) Falk, J. E. (1964) *Porphyrins and Metalloporphyrins*, p 236, Elsevier, Amsterdam.
(30) Hargrove, M. S., Barrick, D., and Olson, J. S. (1996) The Association Rate Constant for Heme Binding to Globin Is Independent of Protein Structure. *Biochemistry 35*, 11293–11299.
(31) Gattoni, M., Boffi, A., Sarti, P., and Chiancone, E. (1996) Stability of the heme-globin linkage in ab dimers and isolated chains of human hemoglobin. A study of the heme transfer reaction from the immobilized proteins to albumin. *J. Biol. Chem. 271*, 10130–10136.
(32) Bhakta, M. N., and Wilks, A. (2006) The Mechanism of Heme Transfer from the Cytoplasmic Heme Binding Protein PhuS to the δ-Regioselective Heme Oxygenase of *Pseudomonas aeruginosa*. *Biochemistry 45*, 11642–11649.
(33) Dailey, H. A. (1985) Spectroscopic examination of the active site of bovine ferrochelatase. *Biochemistry. 24*, 1287–1291.
(34) Mulrooney, S. B., and Waskell, L. (2000) High-Level Expression in *Escherichia coli* and Purification of the Membrane-Bound Form of Cytochrome b5. *Protein Expression Purif. 19*, 173–178.
(35) Suits, M. D. L., Jaffer, N., and Jia, Z. (2006) Structure of the *Escherichia coli* O157:H7 Heme Oxygenase ChuS in Complex with Heme and Enzymatic Inactivation by Mutation of the Heme Coordinating Residue His-193. *J. Biol. Chem. 281*, 36776–36782.
(36) Dalton, D. A., del Castillo, L. D., Kahn, M. L., Joyner, S. L., and Chatfield, J. M. (1996) Heterologous Expression and Characterization of Soybean Cytosolic Ascorbate Peroxidase. *Arch. Biochem. Biophys. 328*, 1–8.
(37) Kimoto, H., Matsuyama, H., Yumoto, I., and Yoshimune, K. (2008) Heme content of recombinant catalase from *Psychrobacter* sp. T-3 altered by host *Escherichia coli* cell growth conditions. *Protein Expression Purif. 59*, 357–359.
(38) Li, J. M., Umanoff, H., Proenca, R., Russell, C. S., and Cosloy, S. D. (1988) Cloning of the *Escherichia coli* K-12 *hemB* gene. *J. Bacteriol. 170*, 1021–1025.
(39) Winter, M. B., McLaurin, E. J., Reece, S. Y., Olea, C., Nocera, D. G., and Marletta, M. A. (2010) Ru-Porphyrin Protein Scaffolds for Sensing O2. *J. Am. Chem. Soc. 132*, 5582–5583.
(40) Ortiz de Montellano, P. R. (2010) Catalytic Mechanisms of Heme Peroxidases, in *Biocatalysis Based on Heme Peroxidases* (Torres, E., and Ayala, M., Eds.) Springer-Verlag, Berlin.
(41) Garcia-Arellano, H. (2010) A Compendium of Bio-Physical-Chemical Properties of Peroxidases, in *Biocatalysis Based on Heme Peroxidases* (Torres, E., and Ayala, M., Eds.) Springer-Verlag, Berlin.
(42) Dordick, J. S., Klibanov, A. M., and Marletta, M. A. (1986) Horseradish Peroxidase Catalyzed Hydroxylations: Mechanistic Studies. *Biochemistry 25*, 2946–2951.
(43) Halliwell, B. (1977) Generation of Hydogen Peroxide, Superoxide, and Hydroxyl Radicals during the Oxidation of Dihydroxyfumaric acid by Peroxidase. *Biochem. J. 163*, 441–448.
(44) Casella, L., Gullotti, M., Selvaggini, C., Poli, S., Beringhelli, T., and Marchesini, A. (1994) The Chloroperoxidase-Catalyzed Oxidation of Phenols. Mechanism, Selectivity, and Characterization of Enzyme-Substrate Complexes. *Biochemistry 33*, 6377–6386.
(45) Heinecke, J. W., Li, W., Daehnke, H. L., and Goldstein, J. A. (1993) Dityrosine, a specific marker of oxidation, is synthesized by the myeloperoxidase-hydrogen peroxide system of human neutrophils and macrophages. *J. Biol. Chem. 268*, 4069–4077.
(46) Rittle, J., and Green, M. T. (2010) Cytochrome P450 Compound I: Capture, Characterization, and C-H Bond Activation Kinetics. *Science 330*, 933–937.
(47) Matsunaga, I., Sumimoto, T., Ayata, M., and Ogura, H. (2002) Functional modulation of a peroxygenase cytochrome P450: novel insight into the mechanisms of peroxygenase and peroxidase enzymes. *FEBS Lett. 528*, 90–94.
(48) Groves, J. T. (2003) The bioinorganic chemistry of iron in oxygenases and supramolecular assemblies. *Proc. Natl. Acad. Sci. U. S. A. 100*, 3569–3574.
(49) Wang, Y., Hirao, H., Chen, H., Onaka, H., Nagano, S., and Shaik, S. (2008) Electron Transfer Activation of Chromopyrrolic Acid by Cytochrome P450 En Route to the Formation of an Antitumor Indolocarbazole Derivative: Theory Supports Experiment. *J. Am. Chem. Soc. 130*, 7170–7171.
(50) de Visser, S. P., and Shaik, S. (2003) A Proton-Shuttle Mechanism Mediated by the Porphyrin in Benzene Hydroxylation by Cytochrome P450 Enzymes. *J. Am. Chem. Soc. 125*, 7413–7424.
(51) Passardi, F., Theiler, G., Zamocky, M., Cosio, C., Rouhier, N., Teixera, F., Margis-Pinheiro, M., Ioannidis, V., Penel, C., Falquet, L., and Dunand, C. (2007) PeroxiBase: The peroxidase database. *Phytochemicals 68*, 1605–1611.

(52) Kunishima, N., Fukuyama, K., Wakabayashi, S., Sumida, M., Takaya, M., Shibano, Y., Amachi, T., and Matsubara, H. (1993) Crystallization and preliminary X-ray diffraction studies of peroxidase from a fungus *Arthromyces ramosus*. *Proteins: Struct. Funct. Bioinf. 15*, 216−220.
(53) Patterson, W. R., and Poulos, T. L. (1995) Crystal structure of recombinant pea cytosolic ascorbate peroxidase. *Biochemistry 34*, 4331−4341.
(54) Gajhede, M., Schuller, D., Henriksen, A., Smith, A. T., and Poulos, T. L. (1997) Crystal Structure of Horseradish Peroxidase C at 2.15 A resolution. *Nat. Struct. Biol. 4*, 1032−1038.
(55) Zámocký, M., Furtmüller, P. G., and Obinger, C. (2010) Evolution of structure and function of Class I peroxidases. *Arch. Biochem. Biophys. 500*, 45−57.
(56) Valderrama, B. (2010) Deactivation of Hemeperoxidases by Hydrogen Peroxide: Focus on Compound III, in *Biocatalysis Based on Heme Peroxidases* (Torres, E., and Ayala, M., Eds.) Springer-Verlag, Berlin.
(57) Feducia, J., Dumarieh, R., Gilvey, L. B., Smirnova, T., Franzen, S., and Ghiladi, R. A. (2009) Characterization of Dehaloperoxidase Compound ES and Its Reactivity with Trihalophenols. *Biochemistry 48*, 995−1005.
(58) Gumiero, A., Murphy, E., Metcalfe, C. L., Moody, P., and Raven, E. L. (2010) An analysis of substrate binding interactions in the heme peroxidase enzymes: A structural perspective. *Arch. Biochem. Biophys. 500*, 13−20.